CORE
Metadata, citation and similar papers at core.ac.uk
Provided by DSpace@MIT

The Astrophysical Journal, 716:504–509, 2010 June 10 doi:10.1088/0004-637X/716/1/504
© 2010. The American Astronomical Society. All rights reserved. Printed in the U.S.A.

# INFLOW–OUTFLOW MODEL WITH CONDUCTION AND SELF-CONSISTENT FEEDING FOR Sgr A*

Roman V. Shcherbakov[1,3] and Frederick K. Baganoff[2]
[1] Harvard-Smithsonian Center for Astrophysics, 60 Garden Street, Cambridge, MA 02138, USA
[2] Center for Space Research, Massachusetts Institute of Technology, Cambridge, MA 02139, USA; rshcherbakov@cfa.harvard.edu
*Received 2009 December 24; accepted 2010 April 26; published 2010 May 19*

## ABSTRACT

We propose a two-temperature radial inflow–outflow model near Sgr A* with self-consistent feeding and conduction. Stellar winds from individual stars are considered to find the rates of mass injection and energy injection. These source terms help to partially eliminate the boundary conditions on the inflow. Electron thermal conduction is crucial for inhibiting the accretion. Energy diffuses out from several gravitational radii, unbinding more gas at several arcseconds and limiting the accretion rate to <1% of Bondi rate. We successfully fit the X-ray surface brightness profile found from the extensive *Chandra* observations and reveal the X-ray point source in the center. The super-resolution technique allows us to infer the presence and estimate the unabsorbed luminosity $L \approx 4 \times 10^{32}$ erg s$^{-1}$ of the point source. The employed relativistic heat capacity and direct heating of electrons naturally lead to low electron temperature $T_e \approx 4 \times 10^{10}$ K near the black hole. Within the same model, we fit 86 GHz optically thick emission and obtain the order of magnitude agreement of Faraday rotation measure, thus achieving a single accretion model suitable at all radii.

*Key words:* accretion, accretion disks – conduction – Galaxy: center – stars: winds, outflows

*Online-only material:* color figures

## 1. INTRODUCTION

Our Galaxy hosts a supermassive black hole (BH) with a mass $M = 4.5 \times 10^6\, M_\odot$ (Ghez et al. 2008; Reid et al. 2008) at a distance $R = 8.4$ kpc. The BH exhibits low luminosity state probably due to inefficient feeding and cooling. Almost all available matter outflows from the region, whereas only the small fraction accretes (Quataert 2004). This feeding region within several arcseconds contains X-ray emitting gas, but some X-rays are expected from a synchrotron self-Compton (SSC) or synchrotron source from accretion at several Schwarzschild radii $r_g$. The study of X-rays offers a unique opportunity to test the full range of accretion scales from several "to $r_g = 10^{-5}$" and construct a single model.

Modeling the accretion flow with such a huge range of scales is a challenge. Three-dimensional (3D) smoothed particle hydrodynamic simulations are performed in the outer region between $1''$ and $10''$ (Rockefeller et al. 2004; Cuadra et al. 2008). Latest magnetohydrodynamic simulations (Sharma et al. 2008) are limited to 3 orders of magnitude in radius and axial symmetry. Only the one-dimensional (1D) calculation (Quataert 2004) can in principle resolve the flow everywhere. Thus, 1D modeling is the approach we adopt extending it down to the BH horizon.

We analyze the quiescent observations (Muno et al. 2008) of X-ray emission from central several arcseconds around Sgr A* in Section 2. The total exposure is 25 times longer compared to previously analyzed data (Baganoff et al. 2003). The super-resolution processing based on spacecraft dithering helps resolving sub-pixel scales. The up-to-date data on stellar wind emitters are summarized in Section 3. We smooth matter ejection rates of individual stars over radius and sum them into a single feeding rate, also properly averaging the wind velocity. This presents a significant improvement over an ad hoc feeding in Quataert (2004). The dynamical two-temperature equations are derived in Section 4. We consider the electron conduction the main energy transport mechanism approximating the unsaturated heat flux by a simple formula. The Bondi flow (Bondi 1952) without heat transport overestimates the X-ray luminosity by a factor of $10^3$. The other important effects considered are the relativistic heat capacity of electrons and superadiabatic heating equivalent to entropy production. The ways to solve the resulting system of equations and corresponding results are presented in Section 5. We employ the shooting method and find the minimum $\chi^2$ fit for the X-ray surface brightness profile, simultaneously fitting 86 GHz flux. The best-fit model requires X-ray point source. The viability of a non-cooling radial flow is examined.

## 2. OBSERVATIONS

Central several arcseconds of the Galaxy were observed quite often over the past several years. The rich region contains point sources identified as X-ray binaries (Muno et al. 2009) and extended emission features (Muno et al. 2008) together with the source coincident with Sgr A*. The latter is expected from hot accreting gas, and source confusion is practically impossible (Baganoff et al. 2003). Sgr A* source exhibits significant X-ray flares associated with the SSC mechanism (Baganoff et al. 2001) or synchrotron (Dodds-Eden et al. 2009). We are interested in quiescent emission, so we exclude the flaring state. We bin the observations in 628 s as a compromise between the time resolution and the number of counts. About four photons on average are received during 628 s and we take only the observations with less than 15 photons, thereby accumulating 953 ks in the quiescent state. The quiescent state also produces some point source X-rays, likely associated with SSC (Moscibrodzka et al. 2009). We model these by a point-spread function (PSF)-broadened central point source. We eliminate the emission from the point sources and bright extended sources offset from Sgr A* (see Figure 1). The bright extended emission may arise from the colliding winds of two strong close emitters or from the collision of hot outflowing

[3] http://www.cfa.harvard.edu/~rshcherb/

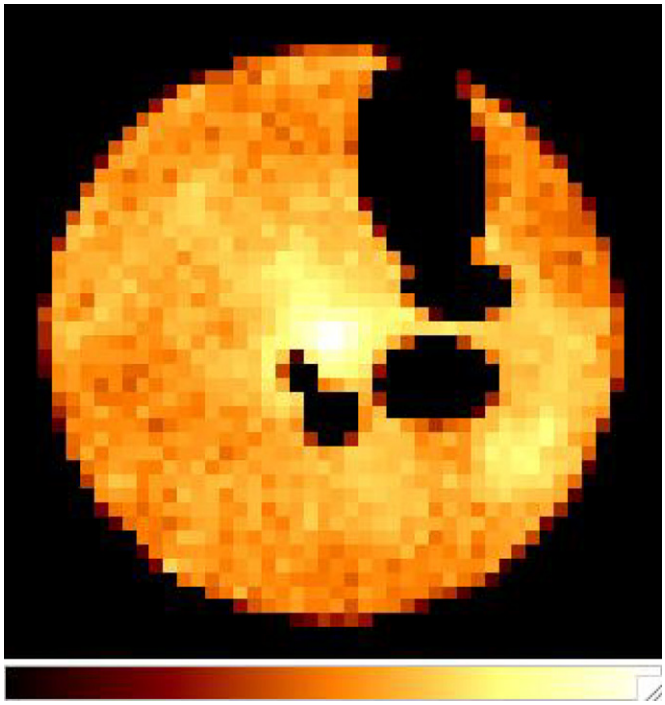

**Figure 1.** *Chandra* image of central 6″ around Sgr A*. Point sources and strong extended features are subtracted.

(A color version of this figure is available in the online journal.)

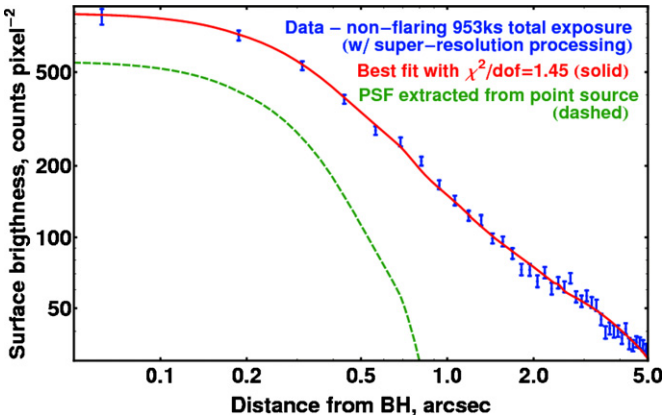


**Figure 2.** Observed radial surface brightness profile (error bars), best fit (solid), and the point source contribution to emission (dashed). The point source contribution is the scaled PSF.

(A color version of this figure is available in the online journal.)

material with cold molecular material. We exclude both effects from modeling of an averaged flow pattern.

We construct the surface brightness profile in counts per pixel squared for the duration of observation as a function of distance from the BH. The size of *Chandra* pixel is 0.″5, which may seem to pose a limit on radial binning of brightness profile. However, the position of satellite is not steady over the duration of observations but is findable with the 0.″1 accuracy by comparing with the known positions of bright point sources. Then we can achieve 0.″1 super-resolution accuracy in the surface brightness profile from knowing the orientation of the detector pixels at any given time. The final profile is shown in Figure 2 (error bars) together with the PSF (dashed) found from the nearby point source J174540.9−290014 (Muno et al. 2009). The PSF is scaled to match the contribution from the point source. The counts cease to be monotonic at about 5″ due probably to the production of X-rays in collisions of cold and hot regions. Therefore, only radiation within the central 5″ is to be modeled. As we are interested in how symmetric the surface brightness profile is, we divide the emitting region into four sectors 90° each centered on Sgr A* and extract the surface brightness profile in each sector. The standard deviation of counts between sectors is below $2\sigma$ the noise within 5″, but rises to several $\sigma$ outward from 5″. This justifies our choice of the outer radiation boundary and proves the applicability of the radial model. Let us now look in more details on manufacturing of the X-ray emitting gas.

## 3. STELLAR WINDS FEEDING

The Galactic Center region has a concentration of massive Wolf-Rayet and blue giant stars, expelling strong winds from their surfaces (Martins et al. 2007). As the strongest wind emitters are usually the brightest stars, all wind emitters are easily identifiable. We take the latest data on ejection rates and velocities (Martins et al. 2007; Cuadra et al. 2008) and complement them with the orbital parameters of stars (Paumard et al. 2006; Lu et al. 2009). Following Cuadra et al. (2008), we minimize eccentricities for the stars not belonging to the stellar disks as identified by Lu et al. (2009). The wind speeds $v_w$ and ejection rates are taken directly from Cuadra et al. (2008).

There are several ways to treat the winds. Rockefeller et al. (2004) performed a simulation with winds from steady stars, whereas Cuadra et al. (2008) considered moving stars. In both cases, the time to reach the quasi-steady solution 300–1000 yr is comparable to or longer than the orbital period at the stagnation point 350 yr. Thus, it is reasonable to average over stellar orbits in a search for a steady-state prescription of feeding. We reconstruct the full 3D orbits, but retain only the apocenter and pericenter distances for the stars. We smooth the total wind ejection rate for each star over the radial extent of its orbit and then smooth with the narrow Gaussian filter to eliminate the divergences at the turning points. We add the resultant feeding profiles together to obtain the total feeding rate as a function of radius (see Figure 3). We square average the wind velocities weighing the contribution of each star by its mass-loss rate. However, the winds also acquire the velocity of a star as viewed by a distant observer. We neglect stars' proper motions in calculations of wind energy. They are negligible at several arcseconds, but would rather contribute to the angular velocity of matter within 1″, where feeding is dominated by few stars. The dependence of the averaged wind speed on radius is shown in Figure 3. Quataert (2004) assumed the power-law mass injection rate $q(r) \propto r^{-\eta}$ for $r \in [2'', 10'']$. The power-law index $\eta = 2$ corresponds to zero slope of $\dot{M}(r) \propto r^2 q(r)$ (see Figure 3) and agrees better with the present calculations, whereas their choice of constant wind velocity does not agree with the present estimate.

We also incorporate S02 star (Martins et al. 2008) into the calculations. The mass-loss rate $\dot{M}_{S02} = 6 \times 10^{-8}\, M_\odot\,\mathrm{year}^{-1}$ of S02 is taken to coincide with that of $\tau$ Sco. S02 has a spectral type $B0 - 2.5V$ and a mass $M \approx 16\, M_\odot$ (Mokiem et al. 2005; Martins et al. 2008), whereas $\tau$ Sco has a very close type $B0.2V$ and a mass $M \approx 15\, M_\odot$ (Mokiem et al. 2005). The inferred accretion rate onto the BH (Sharma et al. 2007a, 2007b) $3 \times 10^{-8}\, M_\odot\,\mathrm{year}^{-1}$ is actually smaller than $\dot{M}_{S02}$, thus the whole accreted material can in principle be provided by a single weak wind emitter. This result is very different from Cuadra et al. (2008), who assumed that all the matter accretes

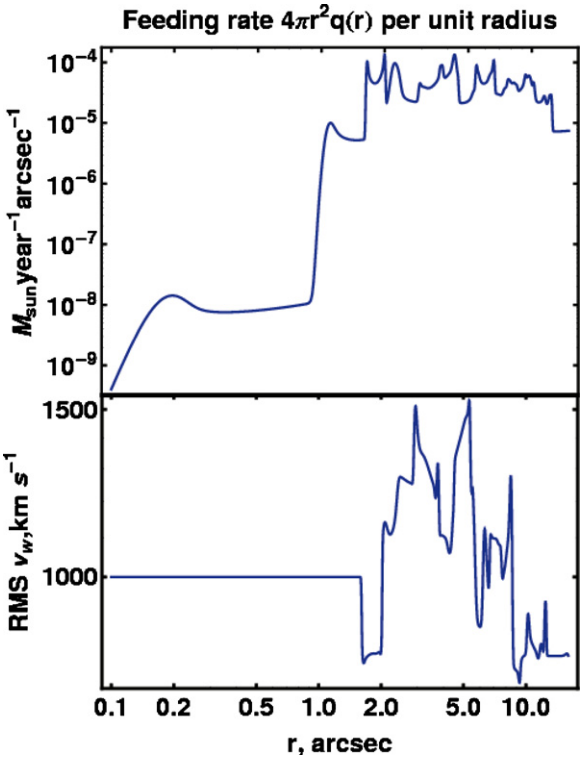


**Figure 3.** Mass input into the feeding region around the BH on the upper panel. Square averaged wind velocity $v_w$ on the lower panel. Feeding is averaged over stellar orbits. Each wiggle represents a turning point of a single orbit. Only S02 star feeds matter within 0.″8.

(A color version of this figure is available in the online journal.)

from the inner boundary of the simulation, thus obtaining in a simplified treatment a much larger accretion rate. However, the direct feeding mechanism (Loeb 2004) by S02 does not work, as its revised $\dot{M}_{S02}$ is much below the value required for feeding without the angular momentum. In turn, the direct feeding by IRS 13E3 (Moscibrodzka et al. 2006) produces too large accretion rate in the absence of conduction.

## 4. DYNAMICAL EQUATIONS

### 4.1. Energy Transport Mechanism

Radiatively inefficient flows can be mediated significantly by the energy transfer from the inner regions to the outer (Blandford & Begelman 1999; Johnson & Quataert 2007; Sharma et al. 2008). Such transfer happens in two distinct ways: via convection or via diffusive energy transport. Convection is seen in numerical simulations. It happens via Alfven instability (Igumenshchev 2006) and magneto-thermal instability (MTI; Sharma et al. 2008) and modifies the density profile. Let us show that the electron heat conduction wins over convection in the accretion flow. First, the MTI is driven by thermal conduction, at any moment the electron conduction flux is larger then the MTI-induced heat flux. Convection implies the motion of large-scale magnetized eddies, which in turn split into smaller eddies and develop the whole turbulent cascade. In such settings the electron conduction is only inhibited a factor of ∼5 (Narayan & Medvedev 2001). The speed of electrons is a factor of $\sqrt{m_p/m_e}$ larger than the sound speed and the convection is subsonic; the same factor lowers the ion diffusive heat transport. The relative strength of convective heat flux is proportional to the gradient of logarithmic entropy, which is normally weaker than the proportionality to the gradient of logarithmic temperature of conductive flux. Combining both effects we conclude that, if there is convection or diffusion, then there is stronger conduction. Severe inhibition of electron conduction happens, if the turbulent cascade does not develop and mixing is absent. This is not the case when the gas accretes. The strength of turbulent magnetic field increases then in the convergent flow leading to dissipation and effective mixing (Shvartsman 1971; Shcherbakov 2008). It is reasonable to think that the whole turbulent cascade develops and the electrons relatively freely find their way around magnetic field lines to connect the different regions of the flow. When the electrons and ions get decoupled from each other, the ion entropy may get equilibrated by convection, whereas the electron temperature levels due to conduction. The investigation of this possibility is left for future research. In present paper, we take the energy transport to happen solely via electron conduction.

There are several different regimes of conduction. First, the collisionality of the flow changes from the large radii to the inner radii as the mean free path of particles $l$ exceeds the flow size $r$. As the flow gets only weakly collisional at several arcseconds, the conductivity is well approximated by a collisionless formula with $\kappa \propto r$. Another assumption of the kind deals with the electron velocity. As electrons can get only mildly relativistic, we take conductivity to be proportional to square root of electron temperature $\kappa \propto \sqrt{T_e}$, instead of proportionality to relativistic electron velocity $\kappa \propto v_c$ (Johnson & Quataert 2007). When the gradient of electron temperature gets too large, the electrons transport heat via a constant saturated flux instead of the flux proportional to the gradient of temperature (Cowie & McKee 1977). We check a posteriori that the flow is in an unsaturated heat flux regime. Finally, we have for the heat flux $Q = -\kappa k_B dT_e/dr$

$$\kappa = 0.1\sqrt{k_B T_e/m_e} r n, \quad (1)$$

where $n = n_e$ is the electron density (Cowie & McKee 1977).

### 4.2. System of Equations

Gravitational energy of gas in the potential of an accretor is the ultimate inflow driver. It gets transformed directly in several types: kinetic energy of bulk toroidal and radial motion, energy of turbulent magnetic and velocity fields, and thermal energy. Turbulent energy can also originate from the toroidal shearing flow in a disk. Turbulence dissipates into thermal motions of ions and electrons on the dynamical timescale, whereas ions and electrons exchange energy by slow Coulomb collisions. The faster collective modes of ion–electron energy exchange may exist, though they may not lead to equilibration of temperatures (Shkarofsky et al. 1966). We do not separate the turbulent term or write an equation on it for the purpose of current work, as its direct dynamical influence is smaller than the influence of additional thermal energy produced via dissipation of turbulence and entropy production (Shcherbakov 2008). Following Johnson & Quataert (2007), we introduce the fractions $f_p$ and $f_e$ of changes of gravitational energy, which go directly into thermal energy of ions and electrons, but relate them via a direct heating mechanism (Sharma et al. 2007a). For the purpose of numerical stability, we enhance Coulomb collisions by a factor of 1000, which effectively makes ion and electron temperatures equal at large distances from the BH, but does not influence $T_e$ near the BH. Let us convert the qualitative ideas into equations.

The composition of plasma determines the exact balance of the BH gravitational pull and supporting gas pressure. Let us

define the source function $q$, so that the ejected mass of stellar winds per second is $\dot{M}_w = \int 4\pi r^2 q dr$. We denote the electron density by $n = n_e$ and write the continuity equation as

$$\frac{\partial n}{\partial t} + \frac{1}{r^2}\frac{\partial (n v_r r^2)}{\partial r} = \frac{q(r)}{\mu_{av}}, \tag{2}$$

where

$$\mu_{\rm av} \approx 1.14 \tag{3}$$

is the average atomic mass per one electron for assumed solar abundance of fully ionized elements (Najarro et al. 2004). The ratio of number densities of atomic nuclei to electrons is

$$d = n_{\rm non-el}/n \approx 0.93. \tag{4}$$

We write separate energy equations for electrons ($e$) and all ions ($p$) in terms of

$$c_{\rm se} = \sqrt{\frac{k_B T_e}{m_p}} \quad \text{and} \quad c_{\rm sp} = \sqrt{\frac{k_B T_p}{m_p}}, \tag{5}$$

assuming all ions have the same temperature. We set the speed of light equal unity $c = 1$ and normalize to it all velocities. The ideal gas law gives normalized gas pressure

$$p_{\rm gas} = p_p + p_e = n\left(c_{\rm se}^2 + d \cdot c_{\rm sp}^2\right) \tag{6}$$

to be substituted into the Euler equation

$$\frac{D v_r}{D t} + \frac{1}{n\mu_{\rm av}}\frac{\partial p_{\rm gas}}{\partial r} + \frac{r_{\rm g}}{2(r-r_{\rm g})^2} + \frac{q(r)}{n\mu_{\rm av}} v_r = 0, \tag{7}$$

where $D/Dt = \partial/\partial t + v_r \partial/\partial r$. The last term corresponds to zero bulk radial velocity of emitted stellar winds.

The electron internal energy density can be approximated as

$$\begin{aligned} u_e &= m_e\left(\frac{3K_3\left(\theta_e^{-1}\right) + K_1\left(\theta_e^{-1}\right)}{4K_2\left(\theta_e^{-1}\right)} - 1\right) \\ &\approx \frac{3}{2}\frac{0.7 + 2c_{\rm se}^2 m_p/m_e}{0.7 + c_{\rm se}^2 m_p/m_e} m_p c_{\rm se}^2. \end{aligned} \tag{8}$$

This takes into account the differential heat capacity of particles (Shkarofsky et al. 1966). The ion internal energy per particle is $u_p = 3/2 m_p c_{\rm sp}^2$.

The energy exchange rate by Coulomb collisions is (Shkarofsky et al. 1966)

$$F_{\rm pe} = 4.3 \times 10^{-19}\frac{n^2}{c_{\rm se}^3}\left(c_{\rm sp}^2 - c_{\rm se}^2\right). \tag{9}$$

The non-relativistic formula is used everywhere, as $F_{\rm pe}$ rate is only significant in the region of non-relativistic electrons. The energy equation for electrons is then

$$\begin{aligned} &n\frac{D}{Dt}\left(\frac{3}{2}\frac{0.7 + 2c_{\rm se}^2 m_p/m_e}{0.7 + c_{\rm se}^2 m_p/m_e} c_{\rm se}^2\right) - c_{\rm se}^2\frac{Dn}{Dt} \\ &\quad = C F_{\rm pe} - f_e n\frac{r_{\rm g} v_r}{2r^2} + \frac{q(1+d)}{2\mu_{\rm av}}\left(\frac{v_r^2}{2} + \frac{v_w^2}{2} - \frac{5}{2}c_{\rm se}^2\right) \\ &\qquad + \frac{1}{r^2}\partial_r\left(r^2\kappa\partial_r c_{\rm se}^2\right), \end{aligned} \tag{10}$$

where $C \sim 1000$ is the enhancement of collisions and conductivity is given by Equation (1). The left-hand side of the Equation (10) represents the compressive heating in the adiabatic flow. The Paczyński–Wiita gravitational potential (Paczyński & Wiita 1980) is implemented for gravitational force, but not in the entropy production term. This reflects the fact that the dissipation of turbulence ceases near the BH as having slower timescale compared to the inflow time. The energy equation for ions reads

$$\begin{aligned} &n\frac{D}{Dt}\left(\frac{3}{2}c_{\rm sp}^2\right) - c_{\rm sp}^2\frac{Dn}{Dt} \\ &\quad = -C F_{\rm pe} - f_p n\frac{r_{\rm g} v_r}{2r^2} + \frac{q(1+d)}{2\mu_{\rm av}}\left(\frac{v_r^2}{2} + \frac{v_w^2}{2} - \frac{5}{2}c_{\rm sp}^2\right). \end{aligned} \tag{11}$$

The energy injection rate into ions is chosen to be the same per electron as the energy injection rate into electrons to facilitate the equality of ion and electron temperatures. Let us write a condition on $f_p$ and $f_e$ to decrease the number of free parameters. We assume the ratio of heating fractions to be given by the direct heating mechanism (Sharma et al. 2007a) as

$$\frac{f_e}{f_p} = \frac{1}{3}\sqrt{\frac{T_e}{T_p}}, \tag{12}$$

despite this calculation is non-relativistic and a large fraction of energy dissipates at the small scales instead of direct large-scale heating.

## 5. SOLUTIONS AND DISCUSSIONS

We solve the derived system of equations from the outer boundary of the feeding region at $14'' = 1.3 \times 10^6 r_{\rm g}$ to the inner boundary at about $1.3 r_{\rm g}$, thus covering 6 orders of magnitude in radius. Such a huge dynamic range requires the special solution technique, the solution of a time-dependent system of equations (Quataert 2004) not being an option. We employ the shooting method and find the smooth transonic solution through the inner sonic point at $\sim 3 r_{\rm g}$. In the presence of conduction the point, where sound speed equals inflow velocity, is not special anymore, and instead the point, where isothermal speed equals the inflow velocity, plays the role of transonic surface (Johnson & Quataert 2007). The system of equations is reduced to one temperature in the outflow by setting $T_e = T_p$ and adding Equations (10) and (11). The inner boundary is set at a point $r_{\rm in}$, where $dT_e/dr = 0$ in a non-conductive solution. Then for any non-zero conductivity the zero heat flux condition $dT_e/dr = 0$ is enforced at $r_{\rm in}$. The outer boundary condition at $r_{\rm out}$ is uncertain. It is natural to think the outflow would be transonic (Lamers & Cassinelli 1999), however, significant outer pressure may hold the gas in the subsonic regime near $r_{\rm out}$. The position of zero velocity stagnation point $r_{\rm st}$ determines the accretion rate $\dot{M}$. Instead of setting the pressure at the outer boundary we regulate that pressure by setting temperature $T_{\rm st}$ at the stagnation point. Thus, we have four independent variables in the fit: accretion rate $\dot{M}$, temperature at stagnation point $T_{\rm st}$, the ion heating rate $f_p$, and the normalization $N$ of the point source contribution. They are all found iteratively to minimize $\chi^2$. We also iteratively find the positions of sonic point and stagnation point. The positions of the inner boundary and the outer boundary are unchanged while solving the four-point boundary value problem.

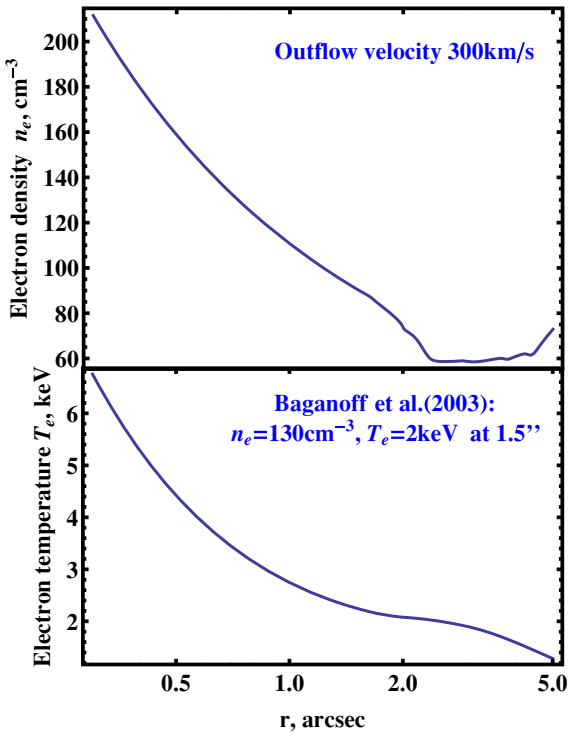


**Figure 4.** Radial profiles of electron density $n = n_e$ in cm $^{-3}$ (upper panel) and electron temperature $T_e$ in keV (lower panel) in the feeding region.
(A color version of this figure is available in the online journal.)

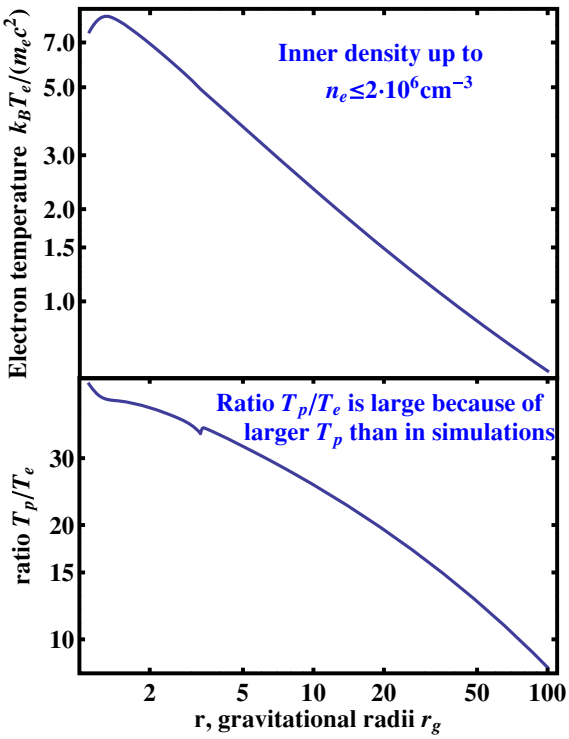


**Figure 5.** Radial profiles of dimensionless electron temperature normalized to electron mass $k_B T_e/(m_e c^2)$ (upper panel) and ratio of ion to electron temperatures $T_p/T_e$ (lower panel) close to the BH. The inner sonic point is at $3r_g$.
(A color version of this figure is available in the online journal.)

The observed surface brightness radial profile is the data we fit. We generate a surface brightness profile corresponding to the dynamical model by performing the optically thin ray tracing of X-rays at a set of photon energies and projected distances from the BH. We employ the up-to-date bremsstrahlung emissivities (Gould 1980 and erratum) and account for the emission by heavy elements, excluding iron. Solar metallicity interstellar absorption (Morrison & McCammon 1983) is assumed with hydrogen column $N_{\rm H} = 10^{23}$ cm$^{-2}$. The fluxes are convolved with the response of *Chandra* to find counts, then blurred with the energy-independent PSF (see Figure 2) and integrated over the radial extent of each bin.

The model with $\dot{M} = 6 \times 10^{-8}\, M_\odot\,{\rm year}^{-1}$, $f_p = 0.46$, $T_{\rm st} = 3.2 \times 10^7$ K, and 550 counts pixel$^{-2}$ produced at $r = 0$ by a point source gives an excellent fit with the minimum reduced $\chi^2 = 1.45$ and weighed $\chi^2_{\rm wei} = 0.68$ with $1/r$ weights. The stagnation point is at $r_{\rm st} = 1\farcs01$. The correspondent unabsorbed point source luminosity $L = 4 \times 10^{32}$ erg s$^{-1}$ is estimated for monoenergetic photons at 4 keV and agrees with the estimates of SSC luminosity in Moscibrodzka et al. (2009). Energy 4 keV is chosen as the energy *Chandra* is most sensitive to for assumed $N_{\rm H}$. The minimum reduced $\chi^2 = 15$ is achieved for the model without the point source. The models with the outer sonic point instead of finite bounding pressure underpredict the X-ray surface brightness at several arcseconds, assuming fixed $N_{\rm H} = 10^{23}$ cm$^{-2}$. The reliable fitting for $N_{\rm H}$ is possible only with the use of spectral data and is left for future research. The assumption $T_p = T_e$ represents the additional point of concern. Temperature equilibrium might not hold at the stagnation point at 1″ (Quataert 2004), however the thermalization rate exceeds the outflow rate at 5″ in our subsonic dense outflow, thus $T_p = T_e$ holds there. The reliable modeling of non-equilibrium flows requires the modeling of the whole spatial structure of the stellar winds and is left for the future research as well.

The profiles of electron density $n_e$ and temperature $T_e$ within several arcseconds from the BH are shown in Figure 4 and compare well with the simple earlier estimates (Baganoff et al. 2003; Quataert 2004). The difference is that our best fit is a subsonic flow supported by the outer medium with the density bounce at 5″. Though the achieved outflow velocity $v_{\rm out} = 300\,{\rm km\,s^{-1}}$ is almost independent of radius for $r > 2''$. The line cooling (Sutherland & Dopita 1993) reduces the heat contents only by several percent for gas reaching 5″, bremsstrahlung cooling being less important.

The profiles of dimensionless electron temperature $k_B T_e/(m_e c^2)$ and ratio $T_p/T_e$ within several Schwarzschild radii from the BH are shown in Figure 5. The electron temperature $T_e = 4 \times 10^{10}$ K and density $n_e = 2 \times 10^6$ cm$^{-3}$ are found close to the BH. This dynamical model gives an excellent fit to the optically thick luminosity $L = 1.73$ Jy at 86 GHz (Krichbaum et al. 2006) for assumed equipartition of thermal energy with the magnetic field. The model overpredicts by a factor of 20 the observed Faraday rotation measure $RM \sim 50\,{\rm cm^{-2}}$ at 230 GHz (Marrone 2007), but this may well be a geometric factor. The accretion rate, temperature, and density near the BH are in good agreement with more complicated models specifically focusing on submillimeter emission (Sharma et al. 2008; Moscibrodzka et al. 2009). We notice that the ratio of ion and electron temperatures $T_p/T_e$ is significantly larger than predicted by Moscibrodzka et al. (2009), but probably because of the significantly lower $T_p$ in their numerical simulations of the limited domain.

The authors are grateful to Ramesh Narayan for fruitful discussions, referee Eliot Quataert, Fu-Guo Xie for encouraging us with the shooting method, Feng Yuan, Jorge Cuadra, and

Avi Loeb for useful comments. The work is supported by the NASA grants NNX08AX04H, NNX08AH32G, Chandra Award GO9-0101X, SAO Award 2834-MIT-SAO-4018, and the NSF grant AST-0805832.

## REFERENCES

Baganoff, F. K., et al. 2001, Nature, 413, 45
Baganoff, F. K., et al. 2003, ApJ, 591, 891
Blandford, R. D., & Begelman, M. C. 1999, MNRAS, 303, L1
Bondi, H. 1952, MNRAS, 112, 195
Cowie, L. L., & McKee, C. F. 1977, ApJ, 211, 135
Cuadra, J., Nayakshin, S., & Martins, F. 2008, MNRAS, 383, 458
Dodds-Eden, K., et al. 2009, ApJ, 698, 676
Ghez, A. M., et al. 2008, ApJ, 689, 1044
Gould, R. J. 1980, ApJ, 238, 1026 (erratum, 243, 677 [1981])
Igumenshchev, I. V. 2006, ApJ, 649, 361
Johnson, B. M., & Quataert, E. 2007, ApJ, 660, 1273
Krichbaum, T. P., Graham, D. A., Bremer, M., Alef, W., Witzel, A., Zensus, J. A., & Eckart, A. 2006, J. Phys: Conf. Ser., 54, 328
Lamers, H. J. G. L. M., & Cassinelli, J. P. 1999, Introduction to Stellar Winds (New York: Cambridge Univ. Press)
Loeb, A. 2004, MNRAS, 350, 725
Lu, J. R., Ghez, A. M., Hornstein, S. D., Morris, M. R., Becklin, E. E., & Matthews, K. 2009, ApJ, 690, 1463
Marrone, D. P., Moran, J. M., Zhao, J., & Rao, R. 2007, ApJ, 654, L57
Martins, F., Genzel, R., Hillier, D. J., Eisenhauer, F., Paumard, T., Gillessen, S., Ott, T., & Trippe, S. 2007, A&A, 468, 233
Martins, F., Gillessen, S., Eisenhauer, F., Genzel, R., Ott, T., & Trippe, S. 2008, ApJ, 672, L119
Mokiem, M. R., de Koter, A., Puls, J., Herrero, A., Najarro, F., & Villamariz, M. R. 2005, A&A, 441, 711
Morrison, R., & McCammon, D. 1983, ApJ, 270, 119
Moscibrodzka, M., Das, T. K., & Czerny, B. 2006, MNRAS, 370, 219
Moscibrodzka, M., Gammie, C. F., Dolence, J. C., Shiokawa, H., & Leung, P. K. 2009, ApJ, 706, 497
Muno, M. P., et al. 2008, ApJ, 673, 251
Muno, M. P., et al. 2009, ApJS, 181, 110
Najarro, F., Figer, D. F., Hillier, D. J., & Kudritzki, R. P. 2004, ApJ, 611, L105
Narayan, R., & Medvedev, M. V. 2001, ApJ, 562, L129
Paczyński, B., & Wiita, P. J. 1980, A&A, 88, 23
Paumard, T., et al. 2006, ApJ, 643, 1011
Quataert, E. 2004, ApJ, 613, 322
Reid, M. J., Broderick, A. E., Loeb, A., Honma, M., & Brunthaler, A. 2008, ApJ, 682, 1041
Rockefeller, G., Fryer, C. L., Melia, F., & Warren, M. S. 2004, ApJ, 604, 662
Sharma, P., Quataert, E., Hammett, G. W., & Stone, J. M. 2007a, ApJ, 667, 714
Sharma, P., Quataert, E., & Stone, J. M. 2007b, ApJ, 671, 1696
Sharma, P., Quataert, E., & Stone, J. M. 2008, MNRAS, 389, 1815
Shcherbakov, R. V. 2008, ApJS, 177, 493
Shkarofsky, I. P., Johnston, T. W., & Bachynski, M. P. 1966, The Particle Kinetics of Plasma (London: Addison-Wesley)
Shvartsman, V. F. 1971, SvA, 15, 377
Sutherland, R. S., & Dopita, M. A. 1993, ApJS, 88, 253